Computational and Theoretical Chemistry 1140 (2018) 125–133

Contents lists available at ScienceDirect

Computational and Theoretical Chemistry

journal homepage: www.elsevier.com/locate/comptc

Electronic structure of isomeric graphene nanoflakes

Cesar Gabriel Vera de la Garza, Gustavo López García, Esaú Martínez Olmedo, Estrella Ramos Peña, Serguei Fomine*

Instituto de Investigaciones en Materiales, Universidad Nacional Autónoma de México, Apartado Postal 70-360, CU, Coyoacán, México, DF 04510, Mexico

ARTICLE INFO

Keywords:
Haeckelite
Hybrid functional
Complete active space
Ionization potential
Electron affinity

ABSTRACT

A comparative theoretical study of graphene nanoflakes (NFs) and isomeric NFs based on two different graphene allotropes has been carried out using hybrid density functional theory and complete active space calculations. Two graphene allotropes **H1** and **H2** consisted of fused azulene rings were found to be less stable compared to isomeric graphene NFs at all theoretical levels. **H1** and **H2** have closed shell singlet ground state independently on their size and strong bond length alternation. For all types of NFs, the evolution of the ionization potential (IP), electron affinity (EA) and band gap (E_g) with size is similar. IP and E_g drop and EA increases with NF size. **H1** and **H2** show lower IPs and E_gs and higher EAs compared to the corresponding graphene NF of the same size. However, IPs, E_gs and EAs converge with size for all three types of the NF becoming nearly identical for the largest representatives of **H1**, **H2** and graphene NF. **H1** and **H2** types of NF have a non-uniform distribution of the electron density across the NF, unlike graphene systems, which makes them promising candidates for regioselective chemical modification.

1. Introduction

Graphene is a monolayer two dimensional (2D) network consisting of the infinite number of fused benzene rings [1]. Since more than a decade graphene has been recognized as a promising and in many aspects revolutionary material for its extraordinary magnetic [2] and electronic [3] properties, namely – extremely high charge carrier mobility, room temperature quantum Hall effect, ambipolar field effect and outstanding mechanical properties [2–8] to mention a few. The exceptional properties of graphene and the need for novel materials have stimulated numerous studies on graphene modification, by introducing chemical defects either by oxidation or by doping with heteroatoms [9,10]. Another approach is the generation of the topological defects such as vacancies and dislocations. The dimensionality reduction is another efficient way for graphene modification [11,12]. Doping with heteroatoms modifies electron affinity (EA) and ionization potentials (IP) of graphene-based materials, while the dimensionality reduction from 2D (graphene) to 1D (graphene nanoribbons) and further to 0D (graphene nanoflakes) introduces a finite band gap (E_g) in graphene-based materials due to quantum confinement effect.

All these modifications still leave intact the principal building block of graphene structure C_6 sp^2 polygon. However, it has been theoretically discovered [13] a variety of possible planar carbon networks based on different types of polygons which could be considered as different allotropic forms of carbon. Most of these carbon allotropes have planar structures, and all of them are less stable than graphene. Their behavior varies from metals to semiconductors according to the density functional tight binding approach (DFTB) calculations.

Among all allotropes described in [13] the structures **H1-2D** and **H2-2D** (Fig. 1) are the most stable and the most chemically relevant. They consisted of fused C5 and C7 polygons, forming 2D planar network of fused azulene rings. Azulene is an isomer of naphthalene and similarly to naphthalene, azulene is an aromatic molecule according to Hückels rule, **H1-2D** and **H2-2D** are the only graphene allotropes with aromatic building blocks. Azulene itself shows strong intramolecular charge transfer and smaller HOMO-LUMO gap compared to its more stable isomer – naphthalene. These two graphene allotropes have been earlier explored within DFTB framework, moreover, **H1-2D** has been studied at general gradient approximation (GGA) level using PBE functional more than 10 years ago [14]. The above-mentioned allotropes are referred to as haeckelites [14]. The fragments of haeckelite structures can be found as topological defects in graphene [15]. They are called Stone-Wales-type defects. These defects can be formed by single electron impact at energies just below the bond dissociation threshold [15]. Therefore, although haeckelites have not been synthesized yet, they are metastable structures with the activation energies of isomerization which are high enough, to make haeckelites metastable at room temperature without rearrangement to graphene. This

* Corresponding author.
E-mail address: fomine@unam.mx (S. Fomine).

https://doi.org/10.1016/j.comptc.2018.08.007
Received 25 June 2018; Received in revised form 8 August 2018; Accepted 10 August 2018
Available online 11 August 2018
2210-271X/ © 2018 Published by Elsevier B.V.

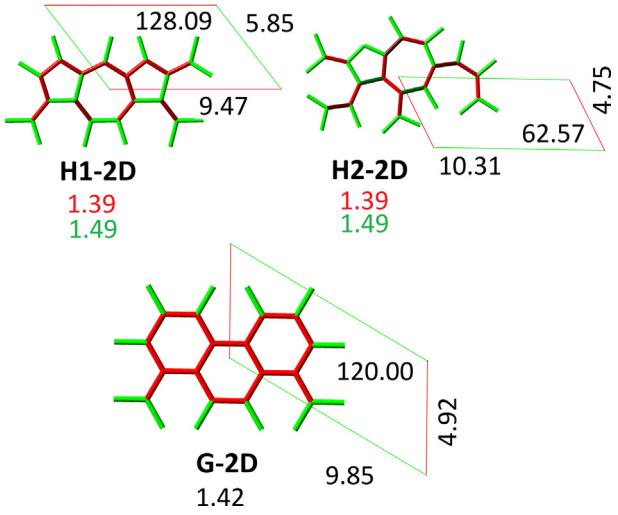

Fig. 1. HSE06/def2-SVP optimized singlet states of two graphene allotropes and graphene supercells. The bond lengths increase from red to green color. The shortest and the longest bond lengths are given in Å. The bond length in graphene is black. Supercell parameters are given in Å and degrees. (For interpretation of the references to colour in this figure legend, the reader is referred to the web version of this article.)

observation is inspiring, since there are no theoretical obstacles to synthesize haeckelites. Unlike graphene, haeckelites are metals according to DFTB and GGA calculations [13,14]. The electronic properties of haeckelites are quite different from those of graphene which opens up a new field of applications for haeckelites. Closely related to haeckelites, 1D fused azulene oligomers, for instance, were found to have a ferromagnetic ground state [16].

As it has been mentioned above, the electronic properties of carbon sp^2 networks depend on their dimensionality. The electronic properties of 0D systems – nanoflakes (NFs) can be tailored by changing their size and shape [17]. The goal of this study is to explore the effect of size on the electronic properties of the NFs derived from these new carbon allotropes (Fig. 1) and to compare them with those of the corresponding graphene NFs.

It is well known that graphene NFs and nanoribbons possess multiconfigurational and sometimes high spin ground states [17–19]. DFTB framework and even GGA are not rigorous enough to correctly describe electronic properties of such systems. We used a combination of hybrid DFT and complete active space (CASSCF) method to explore haeckelite NFs. Hybrid DFT possesses reduced self-interaction error compared with pure or GGA DFT [20]. Self-interaction error is responsible for the overdelocalization problem in conjugated systems. CASSCF takes into account static correlation missed in single reference methods like DFT.

2. Computational details

The geometry optimizations of two haeckelite type NFs and graphene NFs, (Fig. 2) were carried out at by two methods; D3bj [21] dispersion corrected BHandHLYP [22], using Turbomole 7.2 code [23] and screened hybrid functional HSE06 [24] using Gaussian 16 suit of programs [25]. For all calculations was used the same def2-SVP basis set [26]. The electronic structures of three 2D systems; graphene, and 2 haeckelite allotropes (Fig. 2) have been calculated, for the comparison purpose too, using periodic boundary conditions (PBC) method coupled with HSE06 functional. HSE06 functional is very reliable in reproducing (E_g) in semiconductors. Being a hybrid, HSE06 has a reduced self-interaction error [20], which is important for the correct description of the conjugated systems. Moreover, HSE06 functional delivers reliable results not only for the periodic systems but also for small molecules. This is an important point since it makes possible a comparison of PBC results with those for molecules. For all optimized structures including 2D systems, frequency calculations were run to ensure that the found structure is a minimum on the potential energy surface. All structure have positive lowest mode vibrations as can be seen from the Table 1 being structurally stable.

BHandHLYP functional predicts very well geometries of conjugated systems [27]. The adopted model reproduced exactly the carbon–-carbon bond lengths in graphene (1.42 Å, [28]) taking as a model the largest studied graphene NF **G4**. However, given the multireference character of the ground states found in many graphene NFs and polyacenes [18], a single reference method like DFT generally overstabilizes high spin states [29] due to spin contamination, since $< S^2 >$ operator and unrestricted Hamiltonian do not commute. This frequently leads to such an artifact as a high spin ground state. Therefore, the energy evaluation has been carried out using CASSCF single point calculation coupled with 6-31G(d) basis set using BHandHLYP/def2-SVP optimized geometries. The active space of 12 electrons and 12 π orbitals was used for energy evaluation, which was the largest active space computationally practical. Gaussian 16 code was used for CASSCF calculations.

Different spin states of the NFs were optimized at DFT level to locate the ground state. However, CASSCF single point energies were used to determine the ground state. For azulene and naphthalene, the active space was composed of 10 electrons and 10 orbitals, which is a complete π-electron active space for these molecules. For the analysis of the polyradical character of the ground states of the NFs, the Head-Gordon formula (1) has been used [30]

$$N_u = \sum_{i=1}^{M} n_i^2 (2-n_i)^2 \quad (1)$$

where N_u is the number of effectively unpaired electrons, n_i is the occupation of i-*th* natural orbital and M is a total number of active orbitals.

In all cases, the stability analysis of the closed shell singlet wavefunction has been run and in case of found instability, the geometry was reoptimized using unrestricted "open shell singlet" broken symmetry (BS) wavefunction. The E_gs of all NFs have been estimated by two methods; as S0 → S1 excitation energies calculated at the time-dependent (TD) DFT level of theory using new MN15 functional [31] coupled with def2-SVP basis set, and as HOMO-LUMO energy difference from HSE06 calculations. The last method allows direct comparison of E_gs for the NFs and 2D systems. BHandHLYP optimized geometries were used for TD-DFT calculations. This model reproduces very well the lowest excitation energy of nanocene. The S0 → S1 excitation energy predicted with this model is of 1.41 eV, very close to the experimentally observed 1.43 eV [32].

The density of states (DOS) plots were calculated using the Gaussian smearing of the energy levels for each band, followed by a histogram sampling. The Gaussian broadening applied to the eigenvalues is 0.2 eV.

3. Results and discussion

3.1. The ground state nature of haeckelite and graphene nanoflakes

The minimized ground state geometries of the NFs are shown in the Fig. 2. The molecular geometries were optimized for different spin states at BHandHLYP/def2-SVP level to detect the ground state. The results are listed in table 1. BHandHLYP/def2-SVP model predicts very well singlet-triplet (S-T) splitting for naphthalene and azulene (Table 2).

According to the Ovchinnikov rule [33] the total spin of the ground state for alternant conjugated hydrocarbon is $(N_a - N_b)/2$ where N_a and N_b are the numbers of colored (a-type) and uncolored (b-type) atoms. When $N_a = N_b$ as in **Gn** NFs, the ground state must be singlet. The studied carbon allotropies **H1-n** and **H2-n** NFs are different. They

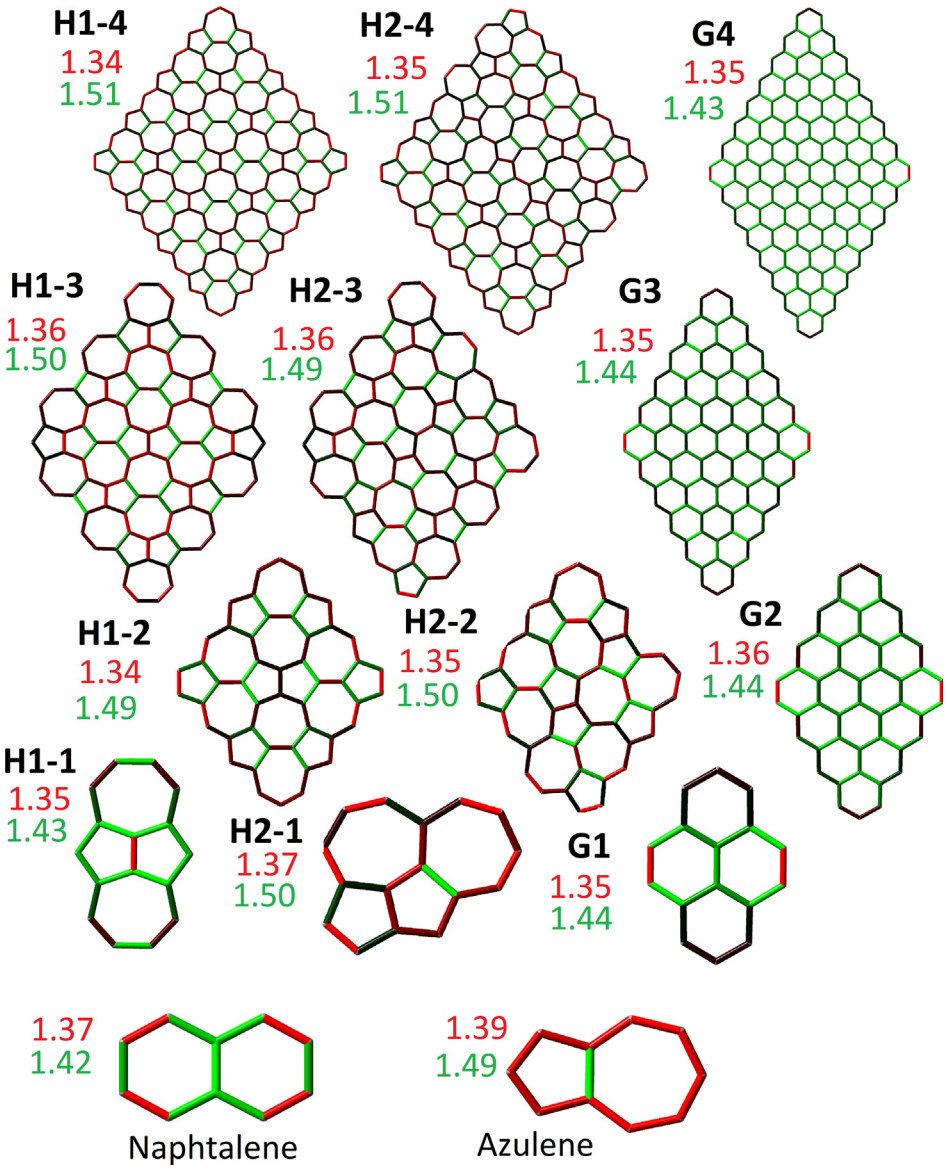

Fig. 2. BHandHlyp/def2-SVP optimized ground state geometries of studied nanoflakes. The bond lengths increase from red to green color. The shortest and the longest bond lengths are given in Å. (For interpretation of the references to colour in this figure legend, the reader is referred to the web version of this article.)

Table 1
The lowest frequency normal vibrations of isomeric graphene nanoflakes including 2D systems optimized at HSE06/def2-SVP level (cm^{-1}).

System	H1-n	H2-n
1	76.4	97.2
2	6.0	19.6
3	15.7[a]	12.1
4	1.36[a]	15.4[a]
2D	130.4	132.2

[a] The structures are not totally plane (Fig. 4).

are not alternant and, therefore, the Ovchinnikov rule does not apply to them. Therefore, there is no way of knowing a priori the nature of their ground states.

For small members of **Gn**, **H1-n** and **H2-n** NFs, where spin contamination is still small (up to **G1**, **H1-2**, and **H2-2**), BHandHLYP/def2-SVP model should deliver reliable S-T splitting. Closed shell singlet was found to be unstable, starting from **G1**, **H1-2**, and **H2-2**, the ground state becomes "open shell singlet"- a result of broken symmetry solution with $M_s = 0$. All larger NFs show very high spin contaminations at BHandHLYP level, even for triplet states, therefore, their relative energies may be unreliable. As seen, BHandHLYP/def2-SVP model predicts singlet state ($M_S = 0$) to be the ground state for all NFs except for **G3**, where triplet state has lower energy. Strong spin contamination is a possible indication of a multiconfigurational character of the wavefunction. Table 2 shows results of single point CASSCF(12,12) calculations for studied NFs using BHandHLYP optimized geometries. As seen, CASSSCF reproduces very well S-T splitting of naphthalene and azulene. Since CASSCF method lacks spin contamination problem and treats qualitatively correctly the multiconfigurational wavefunctions, it reproduces well S-T splitting for multiconfigurational systems. As seen from the Table 2, although S-T splitting decreases with the NF size for all systems, the ground state remains singlet in agreement with the Ovchinnikov rule for Gn NF's [33], unlike DFT artificially overstabilizing triplet states due to spin contamination. Although naphthalene has larger S-T splitting than azulene, S-T splitting decreases more rapidly with size for graphene NFs compared to haeckelite NFs. Especially large S-T splitting is observed for **H2** series, where the difference between triplet and singlet state is higher than 10 kcal/mol, even for the largest **H2-4** NF. Fused aromatic systems like graphene NFs and

Table 2
. Relative energies of singlet ($M_S = 0$) and triplet states ($M_S = 1$) estimated at different theoretical levels and $< S^2 >$ expectation values for DFT solutions.

Molecule	$M_S = 0$	$< S^2 >$	$M_S = 1$	$< S^2 >$
BHandHLYP/def2-SVP				
Naphthalene	0	0	62.6	2.06
G1	0	0	47.8	2.10
G2	0[a]	2.00	10.7	2.30
G3	10.97 [a]	2.68	0	4.63
G4	0[a]	6.76	35.1	5.94
Azulene	0	0	38.3	2.06
H1-1	0	0	36.5	2.07
H1-2	0[a]	0.25	5.92	2.45
H1-3	0[a]	2.28	6.65	2.19
H1-4	0[a]	2.94	0.14	4.33
H2-1	0	0	25.4	2.15
H2-2	0[a]	0.64	7.02	2.32
H2-3	0[a]	0.95	6.78	2.65
H2-4	0[a]	1.60	0.21	3.16
CASSCF/6-31G(d)//BHandHLYP/def2-SVP				
Naphthalene	0	–	63.7	–
G1	0	–	49.3	–
G2	0	–	10.5	–
G3	0	–	4.64	–
G4	0	–	1.19	–
Azulene	0	–	40.1	–
H1-1	0	–	41.8	–
H1-2	0	–	32.7	–
H1-3	0	–	12.9	–
H1-4	0	–	1.73	–
H2-1	0	–	36.8	–
H2-2	0	–	41.7	–
H2-3	0	–	24.5	–
H2-4	0	–	12.4	–

[a] Broken symmetry solution.

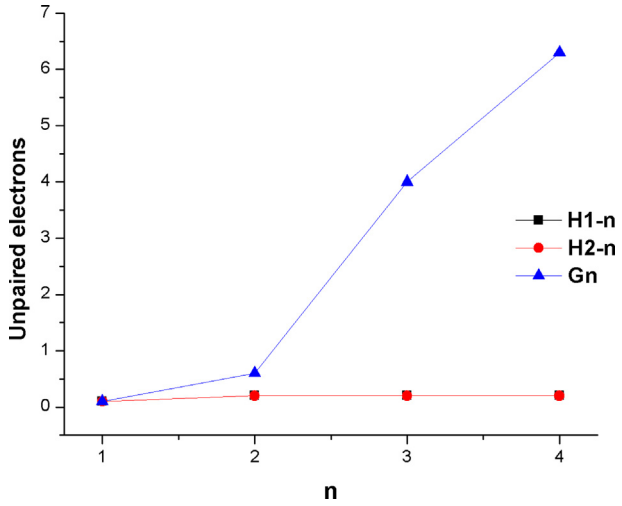

Fig. 3. Occupation numbers of active orbitals in haeckelite and graphene nanoflakes in CASSCF (12, 12)//BHandHLYP/def2-SVP calculations.

polyacenes frequently have polyradical ground states [18,34]. We calculated the number of effectively unpaired electrons for all three types of NFs using the occupations of active orbitals from CASSCF calculations as described in Computational Details section. The results are shown in Fig. 3.

As seen, there is a notable difference between graphene and haeckelite NFs. For graphene NFs the number of effectively unpaired electrons increases rapidly from less than 0.1 for naphthalene to more than 6 for **G4**. NFs **G3** and **G4** have clearly polyradicalic antiferromagnetic ground states. In case of haeckelite NFs **H1-n** and **H2-n**, the situation is very different. In spite of strong spin contamination of BS solutions with $M_s = 0$, the number of effectively unpaired electrons remains low for all NF sizes, being around 0.2. Therefore, unlike graphene NFs, the ground state of both types of haeckelite NFs can be described as closed shell singlet systems.

3.2. The geometry of the nanoflakes and 2D systems

Fig. 2 shows optimized geometries of haeckelite and graphene NFs optimized at dispersion corrected BHandHLYP/def2-SVP method for the spin state with $M_s = 0$. According to the selected color scheme, the shortest bonds are red and the longest are green. As seen from the Fig. 2, the most important difference between haeckelite and graphene NFs is the bond length alternation (BLA) pattern. The BLA is much greater in haeckelite systems compared to graphene ones. BLA pattern in graphene NFs is the most notable at the edges where the formation of the quinoid pattern is clearly seen. The shortest C—C bonds are between 1.35 and 1.36 Å and the largest is between 1.43 and 1.44 Å, independent on the size of the NF. The BLA pattern grows smaller in the center of the graphene NFs, and it decreases even more with the NF size. Thus, for the largest graphene NF, **G4**, the bond lengths in the central benzene rings are close to 1.42 Å, similar to C—C bonds of graphene.

Both **H1-n** and **H2-n** have very different BLA patterns from graphene, resembling that of azulene where the largest bond is the bond that fuses pentagon and heptagon rings. The selected computational model also reproduces very well the experimental bond lengths in azulene [35] where the largest C—C bond is of 1.48 Å. The BLA pattern of the NFs barely depends on the NF size for graphene, however, BLA slightly increases with size for **H1-n** and **H2-n** type of NFs. Similar to graphene NFs, the edge C—C bonds are notably shorter compared to internal ones.

Fig. 1 shows three optimized supercells with the same number of atoms for closed shell singlet state; two 2D allotropes (**H1-2D**, **H2-2D**) and graphene (**G-2D**). The color scheme is similar to Fig. 2. HSE06 functional have been used for the optimization of all 2D structures. According to our test calculations using HSE06 functional, the bond lengths for graphene NFs are 0.01 Å longer compared to the dispersion corrected BHandHLYP model. As seen from the Fig. 1, both graphene allotropes maintain BLA pattern, characteristic of the NFs. Slightly reduced BLA in **H1-2D** and **H2-2D** compared to the corresponding NFs could be related to a smaller fraction of the Hartree-Fock exchange in HSE06 functional, compared to BHandHLYP. On the other hand, graphene shows no BLA pattern at all, with all C—C bond length of 1.42 Å in accordance with the experiment.

The most of the nanoflakes and all 2D systems are structurally stable in their planar form as follows from the frequency analysis, except for **H1-3**, **H1-4** and **H2-4**. Their optimized geometries are shown in Fig. 4. As seen, they are slightly bent. This effect is the most notable for **H1-n**

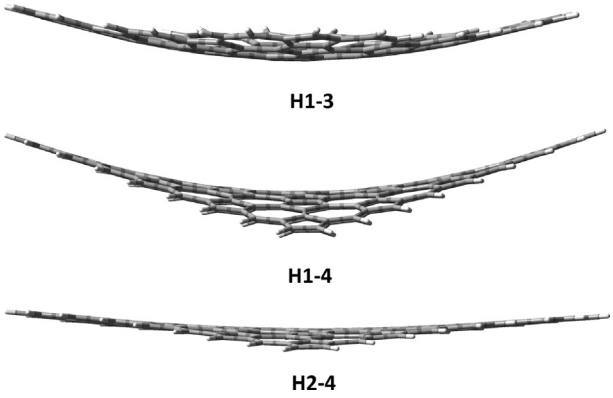

Fig. 4. HSE06/def2-SVP optimized structures of **H1-3**, **H1-4** and **H2-4** nanoflakes.

series and much less for isomeric **H2-n** nanoflake where the largest nanoflake is almost flat. In the case of these three nanoflakes their planar structures have one imaginary frequency, corresponding to out of plane bending vibrations. The energy difference between planar and bent structures for **H1-3**, **H1-4** and **H2-4** are rather small, being of 0.83, 3.99 and 0.06 kcal/mol at HSE06/def2-SVP level of theory, respectively. The most notable difference between planar and bent structure shows **H1-4**, however even in this case the difference between calculated IP and EA for planar and bent structures are less than 0.01 eV. Therefore, we believe that planar structures are good enough for the calculations of the electronic properties.

3.3. The relative stability of haeckelite and graphene nanoflakes

The relative stability of **H1-2D** and **H2-2D** systems have already been estimated using DFTB approach [13] which predicts **H2-2D** to be 3.46 kcal/mol per carbon atom more stable than **H1-2D** and 7.10 kcal/mol per carbon atom less stable than graphene. We have estimated the relative stability of graphene allotropes and the corresponding NFs including azulene and naphthalene at different theoretical levels; HSE06, dispersion corrected BHandHLYP functionals and at CASSCF level, using BHandHLYP optimized geometries. The results are listed in Table 3.

The results of DFTB and hybrid DFT calculations are in qualitative agreement for 2D systems pointing to the **H2-2D** system as the most stable, however, HSE06 functional predicts notably smaller energy difference between two graphene allotropes, only of 0.5 kcal/mol per carbon atom. Similarly, to the prediction of the energy difference between graphene allotropes, HSE06 functional predicts smaller energy difference between graphene and the most stable haeckelite **H2-2D**, (5.9 kcal/mol per carbon atom). The available theoretical data for the relative stability of **H1-2D** and graphene using GGA approximation (PBE functional) in combination with plane wave basis set give 6.0 kcal/mol per carbon atom [14], close to 6.4 kcal/mol per carbon atom estimated in this work with HSE06 functional.

In case of NFs the relative stability depends on the NF size. We included the experimental energy difference between azulene and naphthalene to test our calculation model. HSE06 slightly underestimates the energy difference, while BHandHLYP and CASSCF overestimate it. For large NFs, however, where graphene NFs show notable multireference character of the ground states, CASSCF results seems to be more reliable. For the largest NFs, the results are in qualitative agreement with the results found for 2D systems. All methods predict that **G4** is the most stable NF followed by **H2-4** and then by **H1-4**. For the smallest NFs, **H1-1**, and **H1-2** all methods indicate that **H1-1** is the most stable isomer with the energy difference of only 0.1 kcal/mol per atom. This trend still maintains for the second NF generation. However, HSE06 predicts similar energy for both of them. In the case of third NF generation, both, BHandHLYP and CASSCF point to **H2-3** as the most stable isomer, while HSE06 predicts **H1-3** to be the most stable one.

Table 3
. Energy difference between **H1-n**, **H2-n** and **Gn** NFs including 2D systems (kcal/mol per carbon atom).

System	HSE06/def2-SVP		BHandHLYP/def2-SVP		CASSCF/6-31G(d)	
	H1-n	H2-n	H1-n	H2-n	H1-n	H2-n
Azulene[a]	3.5	3.5	3.9	3.9	5.5	5.5
1	4.3	4.4	4.8	4.9	5.8	5.9
2	3.9	3.9	4.5	4.6	4.2	4.3
3	4.6	4.9	5.2	4.7	5.6	5.0
4	4.6	4.4	5.6	4.7	5.6	5.2
2D	6.4	5.9	–	–	–	–

[a] The experimental energy difference between azulene and naphthalene is 3.7 kcal/mol per carbon atom [41].

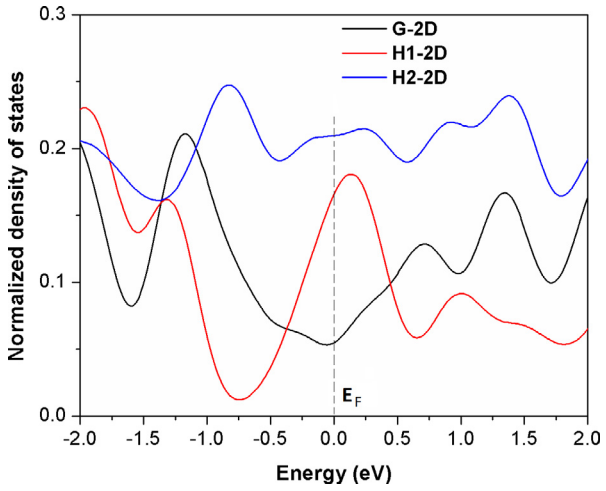

Fig. 5. Normalized density of states (Electrons/eV) against energy (eV) for singlet states from PBC HSE06/def2-SVP calculations for graphene (**G-2D**) and two graphene allotropes (**H1-2D** and **H2-2D**) Energy.

Overall, BHandHLYP and CASSCF seem to deliver more consistent results than HSE06 functional. For small NFs **H1-n** are slightly more stable than **H2-n**. This stability order is changed with size and then maintains for infinite 2D systems.

3.4. Energy gaps, ionization potentials, and electron affinity

The Fig. 5 shows DOS for **H1-2D**, **H2-2D** and graphene as a reference, scaled from 0 to 1 (assigning the 1 for the highest value of DOS for each system). X-axis range is limited to 4 eV near the Fermi level for better viewing.

The results of PBC calculations at HSE06 level agree with the results of DFTB [13] and PBE calculations [14] where both allotropes, **H1-2D** and **H2-2D** were found to be metals. As seen, **H1-2D** and **H2-2D** have non zero density of states at Fermi level, while in case of graphene the density of states is close to 0 at this point. Unlike 2D systems all NFs as expected show finite E_g.

Figs. 6 and 7 show the evolution of E_g with the NF size. The E_gs have been calculated as HOMO-LUMO energy differences of HSE06/def2-SVP optimized structures and also as S0 → S1 excitation energies using BHandHLYP/def2-SVP minimized geometries at TD-MN15/def2-SVP level. Estimated E_gs can be compared with available experimental data for naphthalene (4.35 eV) [36], azulene 2.14 eV [37] and pyrene (3.81 eV) [36] (G1). A simple HOMO-LUMO energy difference overestimates E_g in azulene by some 0.75 eV, underestimates it in case of pyrene by 0.5 eV and reproduces the excitation energies of naphthalene within 0.05 eV. TD-DFT calculations agree much better with experiment, the error for naphthalene, azulene, and pyrene does not exceed 0.3 eV. However, both methods of the E_g determination reveal the similar behavior of E_g with NF size. The E_g decreases with NF size for all systems and **H1-n** and **H2-n** NFs always have smaller E_g than the corresponding **Gn** NFs. This difference, however, decreases with the NF size. While the E_g difference between naphthalene and azulene is of 1.5–2 eV, depending on the estimation method, for the largest NF this difference is reduced to less than 0.5 eV and E_g disappeared completely for graphene and their allotropes, **H1-2D** and **H2-2D**. Both methods: the HOMO-LUMO energy difference and TD-DFT excitation energies; predict very similar behavior for E_g with size for **H1-n** and **H2-n** NF types without any important differences. As seen from the Figs. 6 and 7 there is a very good linear correlation between reciprocal of the number of carbon atoms and E_g for all three NF types and for all calculation methods. The R-squared is more than 0.9 for all NF types and all methods of E_g estimation. This behavior is very similar to that of conjugated polymers [38].

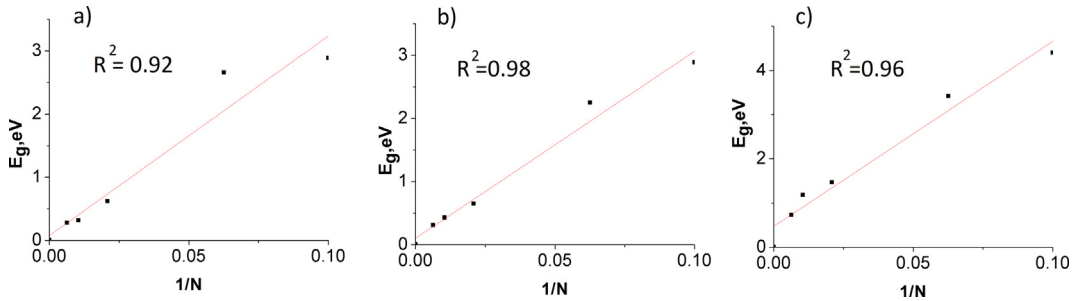

Fig. 6. The band gap (E_g) evolution with the reciprocal of the number of carbon atoms (1/N) for **H1-n** (a), **H2-n** (b) and **Gn** nanoflakes including **H1-2D**, **H2-2D**, and **G-2D** systems, estimated as HOMO-LUMO energy difference at HSE06/def2-SVP level.

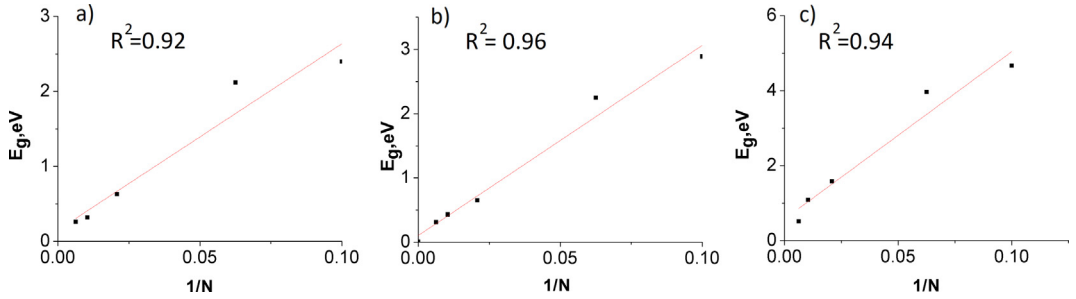

Fig. 7. The band gap (E_g) evolution with the reciprocal of the number of carbon atoms (1/N) for **H1-n** (a), **H2-n** (b) and **Gn** (c) nanoflakes estimated as S0- → S1 excitation energies at TD-MN15/def2-SVP level for dispersion corrected BHandHLYP/def2-SVP optimized geometries.

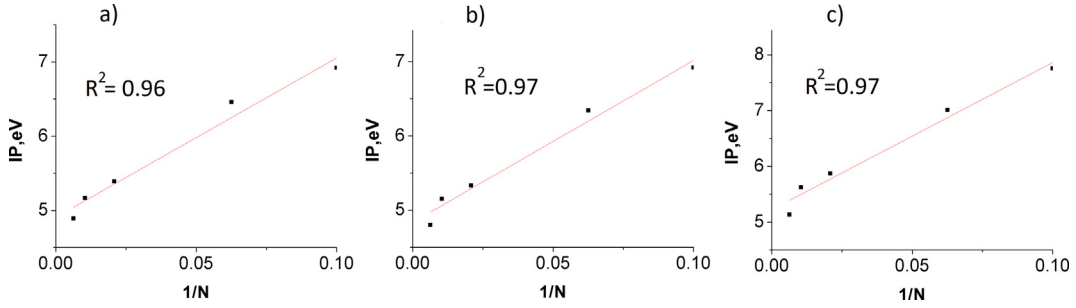

Fig. 8. Ionization potential (IP) evolution with the reciprocal of the number of carbon atoms (1/N) for **H1-n** (a), **H2-n** (b) and **Gn (c)** nanoflakes at BHandHLYP/def2-SVP level of theory.

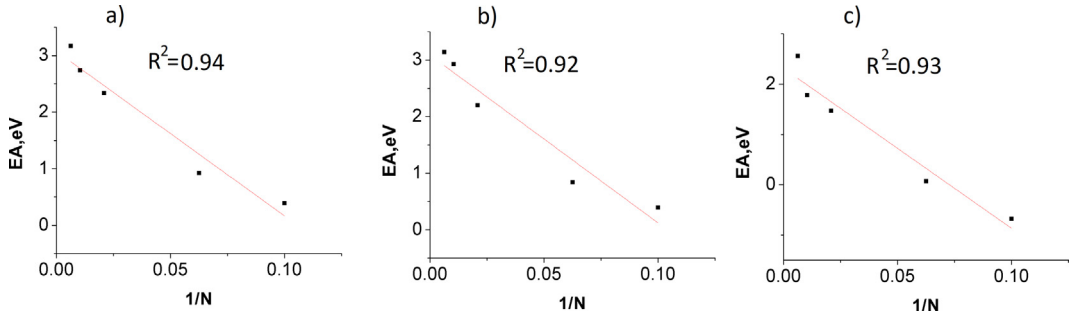

Fig. 9. Electron affinity (EA) evolution with the reciprocal of the number of carbon atoms (1/N) for **H1-n** (a), **H2-n** (b) and **Gn (c)** nanoflakes at dispersion corrected BHandHLYP/def2-SVP level of theory.

Figs. 8 and 9 show the evolution of adiabatic IPs and EAs with the NF size (the reciprocal of the number of atoms). Similar to E_g, there is a good linear correlation (R-squared > 0.9) for both IP and EA with the reciprocal of the number of atoms. For all NF types, EA increases and IP drops with NF size. BHandHLYP/def2-SVP model has been used for the evaluations of IP and EA. This model correctly predicts negative electron affinity for naphthalene [39] and positive one for azulene [40]. Graphene NFs have higher IP and lower EA compared to **H1-n** and **H2-n** NF size, similar to naphthalene compared to azulene. However, in the case of graphene NFs, their IP and EA change faster with size and for the largest NFs **G4**, **H1-4** and **H2-4** IP and EA become very close. This is due to much smaller BLA pattern in graphene NFs compared to **H1-n** and **H2-n** ones leading to more efficient electron delocalization with size. This trend can be clearly seen inspecting HOMOs for cation- and anion-radicals for the largest representatives of the NFs of each type. In these cases, HOMOs follows the delocalization pattern for the cation polarons

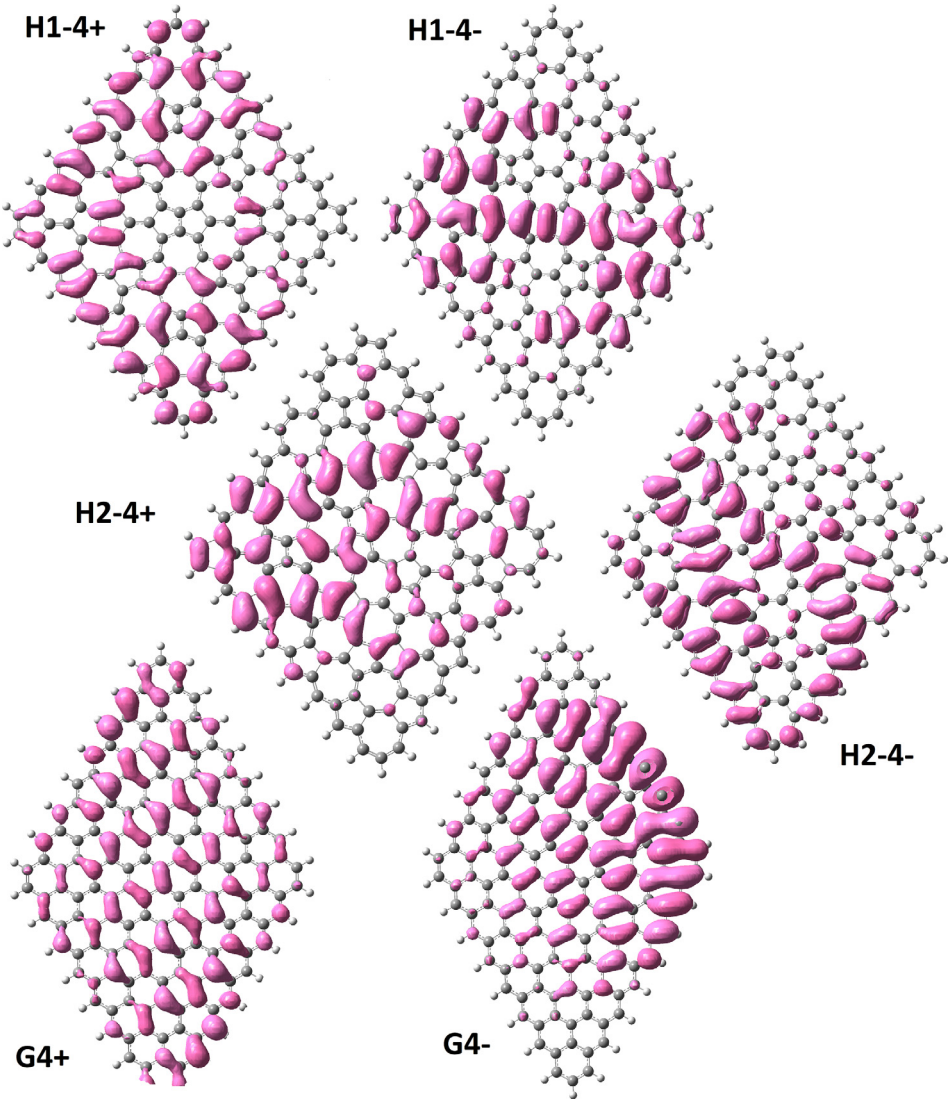

Fig. 10. HOMOs of cation- and anion-radicals of **H1-4** (**H1-4**+ and **H1-4-**), **H2-4** (**H2-4**+ and **H2-4-**) and **G4** (**G4**+ and **G4-**) estimated at dispersion corrected BHandHLYP/def2-SVP level.

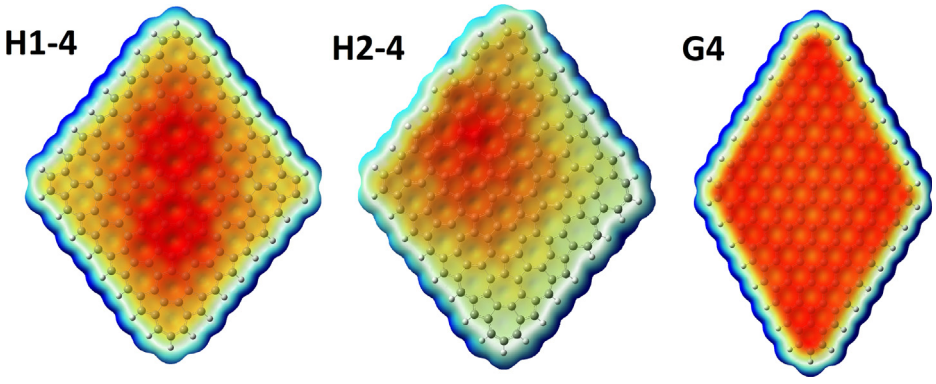

Fig. 11. Electrostatic potential mapped onto total electron density from CASSCF(12,12)/6-31G(d)//BHandHLYP/def2-SVP calculations for singlet states of **H1-4**, **H2-4** and **G4** nanoflakes.

and the polaron anions, respectively.

As seen from the Fig. 10, the delocalization patterns of the cation polaron and the anion polaron in **G4** involve the entire NF, while in the case of **H1-4** and **H2-4**, both HOMO of the cation and anion radicals are more localized. This difference contributes to the slower change of the IP and EA in **H1-n** and **H2-n** NFs compared to **Gn** systems. The electron confinement in the haeckelites NFs can be directly observed from Fig. 11 where the electrostatic potential is mapped onto total electron density for the largest NFs of three different types, as seen from the figure, the electrons are distributed rather uniformly over entire **G4**,

while in the case of **H1-4** and especially **H2-4** the electron distribution is quite different. In case of **H1-4**, the most of the electron density is concentrated in the center of the NF, while in case of **H2-4** the most of electron density is moved off the center of the molecule.

Since **G4** is plane and **H1-4** and **H2-4** are not, we also calculated the electrostatic potential mapped onto total electron density for plane **H1-4** and **H2-4** structures. The non uniform electron distribution for both plane and curved structures are very similar indicating that the origin of this phenomenon is the topological difference between the NF structures and not the curved geometry.

These data reveal the difference between graphene and haeckelite NFs. In graphene, all carbons are in the similar chemical environment which makes it difficult regioselective chemical modification of the graphene NFs. The situation is quite different for haeckelite systems, where there is a different chemical environment for different atoms, as it can be seen from the electrostatic potential maps. This will facilitate regioselective chemical modification of haeckelite NFs.

4. Conclusions

All types of NFs; graphene and haeckelite were shown to have singlet ground states, although singlet-triplet gap drops notably with the NF size. Small NFs of all types have closed shell singlet ground state. The difference between the ground state natures of both NF types becomes evident for large NFs; large graphene NFs have polyradicalic antiferromagnetic ground state, while even large haeckelite NFs maintain closed shell singlet ground state. This difference is originated from BLA pattern. Haeckelite NFs have large BLA independently on their size, while graphene NFs show small BLA pattern.

Graphene NFs are more stable than the corresponding haeckelite ones, **H2-n** being more stable than **H1-n**, in accordance with DFTB data for the infinite 2D systems. The difference in stability between **H1-n** and **H2-n** NFs increases with size. For all types of NFs; **H1-n** and **H2-n**, the evolution of IP, EA and E_g with size is similar. IP and E_g drop and EA increases with size. **H1-n** and **H2-n** show lower IP and E_g and higher EA compared to the corresponding graphene NFs of the same size. However, IP, E_g, and EA converge with size for all three NF types becoming nearly identical for the largest representatives (**G4**, **H1-4**, and **H2-4**).

Unlike graphene NFs, haeckelite systems have a non-uniform distribution of the electron density across the NF, which makes them promising candidates for regioselective chemical modification.

Acknowledgments

We acknowledge the financial support from CONACyT (Grant 251684) and from supercomputing facilities of National Autonomous University of Mexico.

Appendix A. Supplementary material

Supplementary data associated with this article can be found, in the online version, at https://doi.org/10.1016/j.comptc.2018.08.007.

References

[1] K.S. Novoselov, A.K. Geim, S.V. Morozov, D. Jiang, Y. Zhang, S.V. Dubonos, I.V. Grigorieva, A.A. Firsov, Electric field effect in atomically thin carbon films, Science (80-) 306 (2004) 666–669, https://doi.org/10.1126/science.1102896.
[2] E. Kan, Z. Li, J. Yang, Magnetism in graphene systems, Nano 3 (2008) 433–442, https://doi.org/10.1142/S1793292008001350.
[3] A. Castro Neto, F. Guinea, N. Peres, K. Novoselov, A. Geim, The electronic properties of graphene, Rev. Mod. Phys. 81 (2009) 109–162, https://doi.org/10.1103/RevModPhys.81.109.
[4] P. Avouris, Z. Chen, V. Perebeinos, Carbon-based electronics, Nat. Nanotechnol. 2 (2007) 605–615, https://doi.org/10.1038/nnano.2007.300.
[5] M. Dragoman, D. Dragoman, Graphene-based quantum electronics, Prog. Quantum Electron. 33 (2009) 165–214, https://doi.org/10.1016/j.pquantelec.2009.08.001.
[6] A.H. Castro Neto, The carbon new age, Mater. Today 13 (2010) 12–17, https://doi.org/10.1016/S1369-7021(10)70029-8.
[7] C. Lee, X. Wei, J.W. Kysar, J. Hone, Measurement of the elastic properties and intrinsic strength of monolayer graphene, Science 321 (2008) 385–388, https://doi.org/10.1126/science.1157996 Supporting online material.
[8] K.S. Novoselov, Z. Jiang, Y. Zhang, S.V. Morozov, H.L. Stormer, U. Zeitler, J.C. Maan, G.S. Boebinger, P. Kim, A.K. Geim, Room-temperature quantum hall effect in graphene, Science (80-.) 315 (2007) 1379, https://doi.org/10.1126/science.1137201.
[9] M.J. Allen, V.C. Tung, R.B. Kaner, Honeycomb carbon: a review of graphene, Chem. Rev. 110 (2010) 132–145, https://doi.org/10.1021/cr900070d.
[10] D.W. Boukhvalov, M.I. Katsnelson, Chemical functionalization of graphene, J. Phys. Condens. Matter an Inst. Phys. J. 21 (2009) 344205, https://doi.org/10.1088/0953-8984/21/34/344205.
[11] M. Fujita, K. Wakabayashi, K. Nakada, K. Kusakabe, Peculiar localized state at zigzag graphite edge, J. Phys. Soc. Japan 65 (1996) 1920–1923, https://doi.org/10.1143/JPSJ.65.1920.
[12] A.E. Torres, S. Fomine, Electronic structure of graphene nanoribbons doped with nitrogen atoms: a theoretical insight, Phys. Chem. Chem. Phys. 17 (2015) 10608–10614, https://doi.org/10.1039/C5CP00227C.
[13] A.N. Enyashin, A.L. Ivanovskii, Graphene allotropes, Phys. Status Solidi Basic Res. 248 (2011) 1879–1883, https://doi.org/10.1002/pssb.201046583.
[14] X. Rocquefelte, G.-M. Rignanese, V. Meunier, H. Terrones, M. Terrones, J.-C. Charlier, How to identify haeckelite structures: a theoretical study of their electronic and vibrational properties, Nano Lett. 4 (2004) 805–810, https://doi.org/10.1021/nl049879x.
[15] A. Chuvilin, J.C. Meyer, G. Algara-Siller, U. Kaiser, From graphene constrictions to single carbon chains, New J. Phys. 11 (2009), https://doi.org/10.1088/1367-2630/11/8/083019.
[16] Z. Qu, S. Zhang, C. Liu, J.P. Malrieu, Communication: a dramatic transition from nonferromagnet to ferromagnet in finite fused-azulene chain, J. Chem. Phys. 134 (2011), https://doi.org/10.1063/1.3533363.
[17] A.E. Torres, R. Flores, S. Fomine, A comparative study of one and two dimensional π-conjugated systems, Synth. Met. 213 (2016) 78–87, https://doi.org/10.1016/j.synthmet.2016.01.005.
[18] A.E. Torres, P. Guadarrama, S. Fomine, Multiconfigurational character of the ground states of polycyclic aromatic hydrocarbons. A systematic study, J. Mol. Model 20 (2014), https://doi.org/10.1007/s00894-014-2208-6.
[19] G. Trtaquier, N. Suaud, J.P. Malrieu, Theoretical design of high-spin polycyclic hydrocarbons, Chem. – A Eur. J. 16 (2010) 8762–8772, https://doi.org/10.1002/chem.201000044.
[20] R.G. Parr, W. Yang, Density-functional theory of atoms and molecules, 1989. 10.1002/qua.560470107.
[21] S. Grimme, J. Antony, S. Ehrlich, H. Krieg, A consistent and accurate ab initio parametrization of density functional dispersion correction (DFT-D) for the 94 elements H-Pu, J. Chem. Phys. 132 (2010), https://doi.org/10.1063/1.3382344.
[22] A.D. Becke, A new mixing of Hartree-Fock and local density-functional theories, J. Chem. Phys. 98 (1993) 1372–1377, https://doi.org/10.1063/1.464304.
[23] TURBOMOLE V7.2 2017, a development of University of Karlsruhe and Forschungszentrum Karlsruhe GmbH, 1989-2007, TURBOMOLE GmbH, since 2007; available from < http://www.turbomole.com >.
[24] B.G. Janesko, T.M. Henderson, G.E. Scuseria, Screened hybrid density functionals for solid-state chemistry and physics, Phys. Chem. Chem. Phys. 11 (2009) 443–454, https://doi.org/10.1039/B812838C.
[25] M.J.G. Frisch, W. Trucks, H.B. Schlegel, G.E. Scuseria, M.A. Robb, J.R. Cheeseman, G. Scalmani, V. Barone, B. Mennucci, G.A. Petersson, H. Nakatsuji, M. Caricato, X. Li, H.P. Hratchian, A.F. Izmaylov, J. Bloino, G. Zheng, J.L. Sonnenberg, Gaussian 16, Rev. A.03 (2016) (doi:111).
[26] F. Weigend, R. Ahlrichs, Balanced basis sets of split valence, triple zeta valence and quadruple zeta valence quality for H to Rn: design and assessment of accuracy, Phys. Chem. Chem. Phys. 7 (2005) 3297, https://doi.org/10.1039/b508541a.
[27] S. Yang, M. Kertesz, Bond length alternation and energy band gap of polyyne, J. Phys. Chem. A 110 (2006) 9771–9774, https://doi.org/10.1021/jp062701+.
[28] R. Heyrovska, Atomic structures of graphene, benzene and methane with bond lengths as sums of the single, double and resonance bond radii of carbon, arXiv Prepr. arXiv0804.4086. (2008) 1–4. 10.2174/1874199100802010001.
[29] C. Brückner, B. Engels, Benchmarking singlet and triplet excitation energies of molecular semiconductors for singlet fission: tuning the amount of HF exchange and adjusting local correlation to obtain accurate functionals for singlet–triplet gaps, Chem. Phys. 482 (2017) 319–338, https://doi.org/10.1016/j.chemphys.2016.08.023.
[30] M. Head-Gordon, Characterizing unpaired electrons from the one-particle density matrix, Chem. Phys. Lett. 372 (2003) 508–511, https://doi.org/10.1016/S0009-2614(03)00422-6.
[31] H.S. Yu, X. He, S.L. Li, D.G. Truhlar, MN15: A Kohn-Sham global-hybrid exchange–correlation density functional with broad accuracy for multi-reference and single-reference systems and noncovalent interactions, Chem. Sci. 7 (2016) 5032–5051, https://doi.org/10.1039/C6SC00705H.
[32] C. Tönshoff, H.F. Bettinger, Photogeneration of octacene and nonacene, Angew. Chemie – Int. Ed. 49 (2010) 4125–4128, https://doi.org/10.1002/anie.200906355.
[33] A. Ovchinnikov, Multiplicity of the ground state of large alternant organic molecules with conjugated bonds, Theoret. Chim. Acta (Berl.) 47 (1978) 297–304, https://doi.org/10.1007/bf00549259.
[34] F. Plasser, H. Pašalič, M.H. Gerzabek, F. Libisch, R. Reiter, J. Burgdörfer, T. Müller, R. Shepard, H. Lischka, The multiradical character of one- and two-dimensional graphene nanoribbons, Angew. Chemie – Int. Ed. 52 (2013) 2581–2584, https://

doi.org/10.1002/anie.201207671.
[35] J.M. Robertson, H.M.M. Shearer, G.A. Sim, D.G. Watson, Acta Cryst. 15 (1962) 1–8, https://doi.org/10.1107/S0365110X62000018.
[36] J. Ferguson, L.W. Reeves, W.G. Schneider, Vapor absorption spectra and oscillator strengths of naphtalene, anthracene and pyrene, Can. J. Chem. 35 (1957) 1117–1136, https://doi.org/10.1139/v57-152.
[37] A.G. Anderson Jr, B.M. Steckler, J.A.G. Anderson, B.M. Steckler, A Study of the visible absorption spectra and dipole moments of some 1- and 1,3-substituted azulenes, J. Am. Chem. Soc. 81 (1959) 4941–4946, https://doi.org/10.1021/ja01527a046.
[38] R. Gutzler, D.F. Perepichka, π-electron conjugation in two dimensions, J. Am. Chem. Soc. 135 (2013) 16585–16594, https://doi.org/10.1021/ja408355p.
[39] R.S. Beckerr, W.E. Wentworth, Electron affinities and ionization potentials of aromatic hydrocarbons, J. Am. Chem. Soc. 85 (1963) 2210–2214.
[40] N. Ando, M. Mitsui, A. Nakajima, Photoelectron spectroscopy of cluster anions of naphthalene and related aromatic hydrocarbons, J. Chem. Phys. 128 (2008), https://doi.org/10.1063/1.2903473.
[41] J.D. Cox, G. Pilcher, Thermochemistry of organic and organometallic compounds (1970). 10.1002/bbpc.19700740727.